

Transonic Flow Simulation Around the Pitching Airfoil with Accurate Pressure-Based Algorithm

Djavareshkian MH* and Faghihi AR

Faculty of Engineering, Department of Mechanical Engineering, Ferdowsi University of Mashhad, Mashhad, Iran

Abstract

A new pressure based implicit procedure to solve the Euler and Navier-Stokes equations is developed to predict transonic viscous and inviscid flows around the pitching airfoil with high resolution scheme. In this process, nonorthogonal and non moving mesh with collocated finite volume formulation are used. In order to simulate pitching airfoil, oscillation of flow boundary condition is applied. The boundedness criteria for this procedure are determined from Normalized Variable Diagram (NVD) scheme. The procedure incorporates the $k-\varepsilon$ eddy-viscosity turbulence model. In the new algorithm, the computation time is considerably reduced. This process is tested for inviscid and turbulent transonic aerodynamic flows around pitching airfoil. The results are compared with other existing numerical solutions and with experiment data. The comparisons show that the resolution quality of the developed algorithm is considerable.

Keywords: Pitching; Transonic; Inviscid; Viscous; Boundary condition

Nomenclature

A, \tilde{D}, D : Finite difference coefficients

C_1, C_2, C_μ : empirical coefficients

c : chord length

C_l : airfoil lift coefficient

f : physical frequency

K : a factor in SBIC scheme to determine a special scheme

M_∞ : free stream Mach number

u, v : Mean (time-average) velocity components in x and y directions

V : Velocity vector

Γ : Diffusivity coefficient

κ : reduced frequency = $\omega c / (2U_\infty)$

α : angle of attack

\mathcal{E} : Volumetric rate of dissipation

\tilde{a} : Cell face cell

b : one-half of the chord length

C_m : airfoil moment coefficient about quarter chord

F : Flux

I : Flux

K : Kinetic energy of turbulence

T : stress tensor

U_∞ : free stream velocity

Γ_ϕ^t : Turbulent diffusivity coefficients

δv : Cell volume

t : Time

α_m : angle of attack in mean position

ω_a : circular frequency, $2\pi f$

δ_{ij} : Kronecker delta

G : Generation of turbulence kinetic energy

μ : Dynamic viscosity

P : Pressure

σ_ε : Turbulent Prandtl numbers for dissipation rate

θ : angle between mean and moment chords

ρ : Density

R_ε : Reynolds number

μ_t : Turbulent viscosity

σ_k : Turbulent Prandtl numbers for turbulent kinetic energy

ϕ : Scalar quantity

Introduction

In the field of Computational Fluid Dynamics (CFD), there are two categories of numerical methods for simulating moving boundary flow problems. One is the moving grid method [1], which constantly updates the grid according to the position of object. The major limitation of moving grid method is the regeneration of mesh at every time step, which may consume much time and reduce computational efficiency. To overcome this drawback, a pseudo grid-deformation

*Corresponding author: Djavareshkian MH, Faculty of Engineering, Department of Mechanical Engineering, Ferdowsi University of Mashhad, Mashhad, Iran, E-mail: jvareshkian@um.ac.ir

Received April 30, 2013; Accepted June 20, 2013; Published June 28, 2013

Citation: Djavareshkian MH, Faghihi AR (2013) Transonic Flow Simulation around the Pitching Airfoil with Accurate Pressure-Based Algorithm. J Aeronaut Aerospace Eng 2: 112. doi:10.4172/2168-9792.1000112

Copyright: © 2013 Djavareshkian MH, et al. This is an open-access article distributed under the terms of the Creative Commons Attribution License, which permits unrestricted use, distribution, and reproduction in any medium, provided the original author and source are credited.

approach was developed [2]. This approach calculates the grid speed through analytical expression of grid movement. The method is feasible to simulate rotational motion of the object. However, to simulate axial motion of the object, the volume change of grid cells should be considered. Another type of approaches for handling moving boundary problems is the field velocity method [3,4] which adopts the grid speed technique to simulate the velocity change of flow field. This method is especially suitable for calculation of step change of airfoil, and has been successfully applied to calculate the gust response of the airfoil/wing [5-8]. The method of conventional field velocity is usually used to calculate the indicial response by incorporating unsteady flow conditions via grid movement in CFD simulations. The main privilege of this method is direct calculation of aerodynamic responses to step changes in flow conditions. An impulsive change in the angle-of-attack can be considered as an impulsive superposition of a uniform velocity field to the free stream. The magnitude of the indicial change for the angle of attack is used for calculation of the magnitude of normal velocity. In this method, the necessity of uniform distribution of time step over the entire flow domain is guaranteed. In addition, the airfoil is not made to pitch. Hence, the influence of pure angle-of-attack and pitch rate are decoupled efficiently. A similar methodology for simulating responses of an airfoil to step changes in pitch rate and interaction with vertical gusts exists. Moreover, the field velocity method is also applied for prediction of the effects of the trailed vortex wake from the other rotor blades in helicopters, compressors or other turbo machineries. A time dependence study illustrates that a smooth and accurate solution in time requires the consistent evaluation of time metrics in order to satisfy the geometric constitutive law Sitaraman et al. [9].

The objective of the present work is to compute unsteady transonic inviscid and viscous flow fields over a pitching NACA0012 airfoil at various angles of the attack. A new pressure based implicit procedure to solve the Euler and Navier-Stokes equations is developed to predict flow around the pitching airfoil with high resolution scheme. In this process, nonorthogonal and non moving mesh with collocated finite volume formulation are used. In order to simulate pitching airfoil, oscillation of flow boundary condition is applied. The boundedness criteria for this procedure are determined from Normalized Variable Diagram (NVD) scheme. The procedure incorporates the $k-\varepsilon$ eddy-viscosity turbulence model. The algorithm is tested for inviscid and turbulent transonic aerodynamic flows around pitching airfoil. The results are compared with other existing numerical solutions and with experiment data. The comparisons show that the resolution quality of the developed algorithm is considerable.

Governing equations and discretization

The basic equations, which describe conservation of mass, momentum and scalar quantities, can be expressed in Cartesian tensor form as:

$$\frac{\partial}{\partial t}(\rho) + \frac{\partial}{\partial x_i}(\rho u_i) = 0 \quad (1)$$

$$\frac{\partial}{\partial t}(\rho u_i) + \frac{\partial}{\partial x_j}(\rho u_i u_j - T_{ij}) = S_i^u \quad (2)$$

$$\frac{\partial}{\partial t}(\rho \phi) + \frac{\partial}{\partial x_i}(\rho u_i \phi - q_i) = S^\phi \quad (3)$$

The stress tensor and scalar flux vector are usually expressed in terms of basic dependent variable. The stress tensor for a Newtonian fluid is

$$T_{ij} = -\left(P + \frac{2}{3}\mu \frac{\partial u_k}{\partial x_k}\right)\delta_{ij} + \mu\left(\frac{\partial u_i}{\partial x_j} + \frac{\partial u_j}{\partial x_i}\right) \quad (4)$$

The scalar flux vector usually given by the Fourier-type law is

$$q_i = \Gamma_\phi \left(\frac{\partial \phi}{\partial x_i}\right) \quad (5)$$

Turbulence is accounted for by adopting $k-\varepsilon$ turbulence model. The governing

$$\frac{\partial}{\partial t}(\rho k) + \frac{\partial}{\partial x_i}(\rho u_i k - \Gamma_k \frac{\partial k}{\partial x_i}) = G - \rho \varepsilon + D_{comp} + \Theta_{diff} \quad \text{equations for} \quad (6)$$

these quantities are

$$\frac{\partial}{\partial t}(\rho \varepsilon) + \frac{\partial}{\partial x_j}(\rho u_j \varepsilon - \Gamma_\varepsilon \frac{\partial \varepsilon}{\partial x_j}) = C_1 \frac{\varepsilon}{k} G - C_2 \rho \frac{\varepsilon^2}{k} \quad (7)$$

The turbulent viscosity and diffusivity coefficients are defined by

$$\mu_t = C_\mu \rho \frac{k^2}{\varepsilon} \quad (8)$$

$$\Gamma_\phi^t = \left(\frac{\mu_t}{\sigma_\phi^t}\right) \quad (9)$$

and the generation term G in eqs. (6) and (7) is defined by

$$G = \mu_t \left[\left(\frac{\partial u_i}{\partial x_j} + \frac{\partial u_j}{\partial x_i}\right) \frac{\partial u_i}{\partial x_j} - \frac{2}{3} \delta_{ij} \left(\frac{\partial u_m}{\partial x_m} + \rho k\right) \frac{\partial u_i}{\partial x_j} \right] \quad (10)$$

The term D_{comp} and Θ_{diff} are additional $k-\varepsilon$ contributions to the standard model often introduced to account for the effects of compressibility [10,11]. In this work, the models proposed by Yang et al. [10] are adopted, namely,

$$D_{comp} = -\frac{9}{55} k \frac{\partial}{\partial x_i} \left(\frac{\partial}{\partial x_i} - \frac{1}{\rho} \cdot \frac{\partial}{\partial x_i} \right) \frac{\partial}{\partial x_i} \frac{\partial}{\partial x_i}$$

$$\Theta_{diff} = 0$$

The latter being appropriate for high Reynolds number flows, as it is the case here. The values of the turbulence model coefficients used in the present work are given in (Table 1) [10].

The discretization of the above differential equations is carried out using a finite-volume approach. First, the solution domain is divided into a finite number of discrete volumes or cells, where all variables are stored at their geometric centers (Figure 1). The equations are then integrated over all the control volumes by using the Gaussian theorem. The development of the discrete expressions to be presented is effected with reference to only one face of the control volume, namely, e , for the sake of brevity.

For any variable ϕ (which may now also stand for the velocity components), the result of the integration yields

$$\frac{\delta v}{\delta t} [(\rho \phi)_p^{n+1} - (\rho \phi)_p^n] + I_e - I_w + I_n - I_s = S_\phi \delta v$$

Where $I_{(s)}$ are the combined cell-face convection I^c and diffusion I^D fluxes. The diffusion flux is approximated by central differences and

C_1	C_2	C_μ	σ_k	σ_ϵ
1.44	1.92	0.09	1.0	1.3

Table 1: Values of empirical coefficients in the standard k-ε turbulence model.

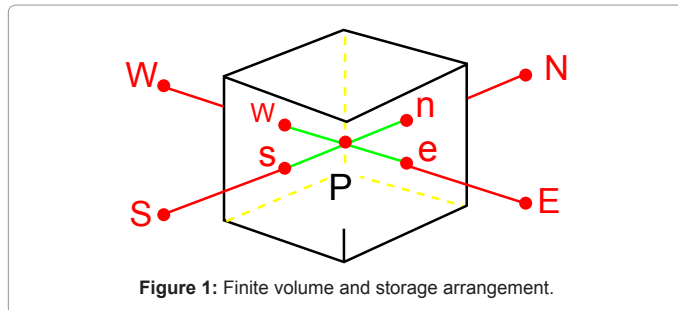


Figure 1: Finite volume and storage arrangement.

can be written for cell-face e of the control volume in Figure 1 as an example as:

$$I_e^D = D_e(\phi_p - \phi_E) - S_e^\phi$$

Where S_e^ϕ stands for cross derivative arising from mesh nonorthogonality. The discretization of the convective flux, however, requires special attention and is the subject of the various schemes developed. A representation of the convective flux for cell-face e is:

$$I_e^C = (\rho \cdot V \cdot A)_e \phi_e = F_e \phi_e$$

The value of the dependent variable ϕ_e is not known and should be estimated using an interpolation procedure, from the values at neighboring grid points. ϕ_e is determined by the SBIC scheme Djavareshkian [12], that it is based on the NVD technique, used for interpolation from the nodes E, P and W. The expression can be written as

$$\phi_e = \phi_w + (\phi_E - \phi_w) \cdot \tilde{\phi}_e$$

The functional relationship used in SBIC scheme for $\tilde{\phi}_e$ is given by

$$\tilde{\phi}_e = \tilde{\phi}_p \text{ if } \tilde{\phi}_p \leq 0 \text{ or } \tilde{\phi}_p \geq 1$$

$$\tilde{\phi}_e = -\frac{\tilde{x}_p - \tilde{x}_e}{K(\tilde{x}_p - 1)} \tilde{\phi}_p^2 + \left(1 + \frac{\tilde{x}_p - \tilde{x}_e}{K(\tilde{x}_p - 1)}\right) \tilde{\phi}_p \text{ if } 0 < \tilde{\phi}_p < K$$

$$\tilde{\phi}_e = \frac{\tilde{x}_p - \tilde{x}_e}{\tilde{x}_p - 1} + \frac{\tilde{x}_e - 1}{\tilde{x}_p - 1} \tilde{\phi}_p \text{ if } K \leq \tilde{\phi}_p < 1 \quad 0 < K \leq 0.5$$

where

$$\tilde{\phi}_{eP} = \frac{\phi_P - \phi_W}{\phi_E - \phi_W} \quad \tilde{\phi}_e = \frac{\phi_e - \phi_W}{\phi_E - \phi_W} \quad \tilde{x}_e = \frac{x_e - x_W}{x_E - x_W} \quad \tilde{x}_p = \frac{x_p - x_W}{x_E - x_W} \quad (19)$$

The limits on the select each value of K could be determined in the following way. Obviously the lower limit is to keep $K=0$, which would represent switching between upwind and central differencing. This should not be favored because; it is essential to avoid the abrupt switching between the schemes in order to achieve the converged solution. The upper limit of K is 0.5, since it represents the constant gradient and there is no need to use anything else than central differencing in that case. The value of K should be kept as low as possible in order to achieve the maximum resolution of the scheme.

According to Eq. (17), if $\tilde{\phi}_P$ (or $\tilde{\phi}_C$ normalized variable at the central node) does not belong to $[0,1]$, the space discretization is first order, otherwise the SBIC scheme has second order accuracy from point of view space discretization. The details of how the interpolation is made is dealt with [12]; it suffices to say that the discretized equations resulting from each approximations take the form:

$$A_p \cdot \phi_p = \sum_{m=E,W,N,S} A_m \cdot \phi_m + S'_\phi$$

Where $A(s)$ are the convection-diffusion coefficients. The term

S'_ϕ in Eq. (19) contains quantities arising from non-orthogonality, numerical dissipation terms, external sources, deferred correction terms, and $(\rho \delta v / \delta t) \phi_p$ of the old time-step/iteration level. For the momentum equations it is easy to separate out the pressure-gradient source from the convected momentum fluxes.

Solution algorithm

The set of Eq. (19) is solved for the primitive variable (velocity components and energy) together with continuity utilizing pressure-based implicit sequential solution methods. The technique used is the PISO scheme presented herein Issa [13]. In this technique, the methodology has to be adapted to handle the way in which the fluxes are computed in Eqs. (15-18). The adapted PISO scheme consists of a predictor and two corrector sequence of steps at every iteration. The predictor step solves the implicit momentum equation using the old pressure field. Thus, for example, for the u component, the momentum predictor stage can be written as

$$u^* = H(u^*) - DVp^o + S'_u$$

Where H contains all terms relating to the surrounding nodes and superscripts $*$ and o denote intermediate and previous iteration values, respectively. Note that the pressure-gradient term is now written out explicitly; it is extruded from the total momentum flux by simple subtraction and addition. The corrector-step equation can be written as

$$u^{**} = H(u^*) - DVp^* + S'_u$$

Hence, from Eqs. (20) and (21)

$$u^{**} - u^* = -DV(p^{**} - p^*) \quad \text{or} \quad \delta u = -DV \delta p$$

Now the continuity equation demands that

$$\frac{\delta \rho}{\delta t} + \nabla \cdot (\rho^* u^{**}) = 0$$

For compressible flows it is essential to account for the effect of change of density on the mass flux as the pressure changes. This is accounted for by linearizing the mass fluxes as flows

$$\rho^* u^{**} \approx \rho^o u^* + \rho^o \delta u + u^* \delta \rho$$

Or

$$\rho^* u^{**} \approx \rho^o u^* - \rho^o DV \delta p + u^* \left(\frac{d\rho}{dp}\right) \delta p$$

Where Eq. (22) is invoked to eliminate δu and $\delta \rho$ is related to δp by the appropriate equation of state. Substitution of Eq. (24) into Eq. (23) yields a pressure-correction equation of the form

$$A_P \cdot \delta p_P^* = A_E \cdot \delta p_E^* + A_W \cdot \delta p_W^* + A_N \cdot \delta p_N^* + A_S \cdot \delta p_S^* + S_P$$

Where S_p is the finite difference analog of $\nabla(\rho^o u^*)$, which vanishes when the solution is converged. The A coefficients in Eq. (25) take the form (the expression for A_E is given as an example)

$$A_E = (\rho^o \tilde{a} D)_e - \lambda_e (\tilde{a} u^*)_e \cdot \left(\frac{d\rho}{dp}\right)_e$$

where λ is a factor whose significance is explained subsequently. The mass flux at a cell face is computed from nodal values of density and velocity, the cell-face values of ρ_e^o and u_e^* in Eq. (26) are not readily available. To compute those values, assumptions concerning the variations of ρ need to be made. In upwinding $\lambda=1$ when u is positive; otherwise it would be zero. Alternatively, in central difference formula $\lambda=1/2$.

Such assumptions have no influence whatsoever on the final solution because they affect only the pressure-correction coefficients, and as δp goes to zero at convergence, the solution is, therefore, independent of how those coefficients are formulated; however, they do influence the convergence behavior.

The structure of the coefficients in Eq. (25) simulates the hyperbolic nature of the equation system. Indeed, a closer inspection of expression

(26) would reveal an upstream bias of the coefficients (A decreases as u increases), and this bias is proportional to the square of the Mach number. Also, note that the coefficients reduce identically to their incompressible form in the limit of zero Mach number.

In the present work, Crank-Nicolson scheme is applied for discretization of time derivative with second order accuracy. This option seems to be the most obvious as it requires the minimum amount of memory storage of the velocity fields. The system of equation is solved by biconjugate gradient method.

New time advancement algorithm

In this research three time advancement algorithms are used for the simulation. Figure 2 shows the flowchart of them. Algorithm 2(a) has external loop to satisfy convergence criteria for each iteration. An internal loop just for pressure equation is used in Figure 2b. The new time advancement algorithm, Figure 2c, is utilized an internal and external loop for calculation.

Boundary conditions

At the inlet of the domain, only three of the four variables need to be prescribed: the total temperature, the angle of attack, and the total pressure. The pressure is obtained by zeroth order extrapolation from interior points. At outlet, the pressure is fixed. Slip boundary conditions are used on the lower and upper walls. In the case of viscous flow, the

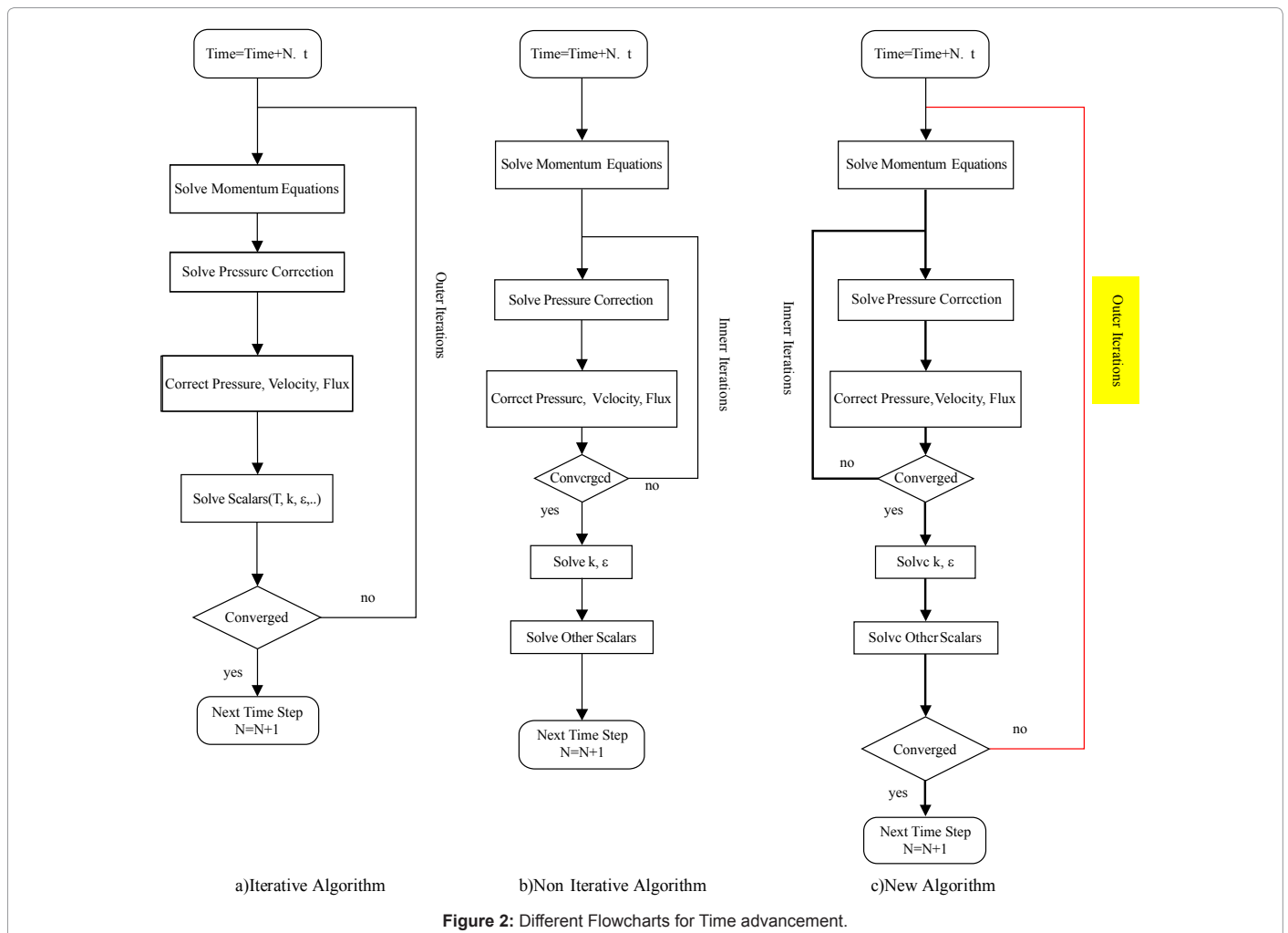


Figure 2: Different Flowcharts for Time advancement.

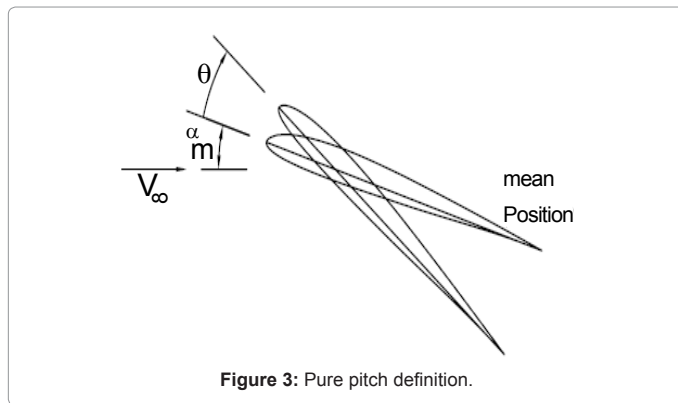


Figure 3: Pure pitch definition.

κ	M_0	α_m (deg.)	α_p (deg.)	c
0.0814	0.755	0.016	2.51	1.0

Table 2: Pure pitch motion parameters.

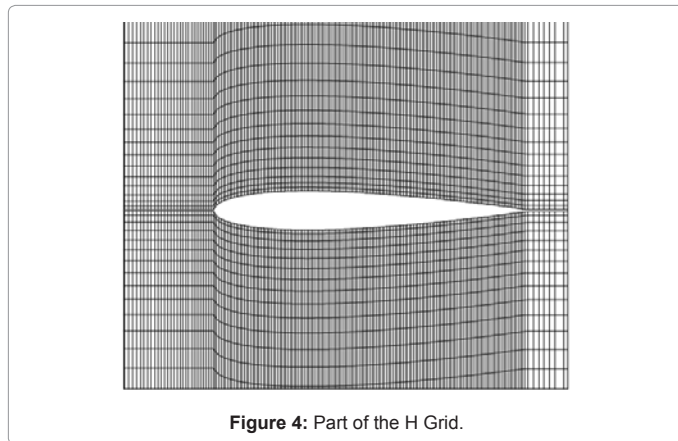


Figure 4: Part of the H Grid.

non-slip condition is applied at the airfoil surfaces. To account for the steep variations in turbulent boundary layers near solid walls, wall functions, which define the velocity profile in the vicinity of no-slip boundaries, are employed. The far-field boundary is set to 30c from the airfoil to minimize its undesired effects on the flow surrounding and is set to slip boundary conditions.

Results and Discussion

In this section, the results of the inviscid and viscous flows over a pitching NACA0012 airfoil along its quarter chord axis are indicated. The simulations are performed at a higher Reynolds number. In particular, we aim to validate the simulation with existing experiment results of a pitching airfoil, and study the lift and drag characteristics of a pitching airfoil. The steady state solutions are used as initial conditions for time-marching calculations. Figure 3 provides an illustration of pure-pitch motion for an airfoil with a mean angle of attack of α_m . The parameters of motion and flow field are described in Table 2. The airfoil is forced into an oscillation around an axis located at the quarter-chord. The angle of attack is specified as:

$$\alpha(t) = \alpha_m + \alpha_p \sin(\omega_\alpha t) \quad (27)$$

The free stream velocities for unsteady computations are set to $u_{inlet} = U_\infty \cos(\alpha(t))$ and $v_{inlet} = U_\infty \sin(\alpha(t))$. An H-type mesh is generated to model the airfoil and the surrounding flow. The schematic of this grid which is used in the present simulation is shown in Figure 4. The

grid dependence test for Navier-Stokes Equation on the NACA0012 airfoil at $M_\infty = 0.755$, $\alpha = -1.8^\circ$ is indicated in Figure 5. Three different mesh sizes were considered: 27680, 57950 and 115960 cells and each simulation emerged from its fully converged solution. Thus the mesh of 57980 cells was selected as a baseline mesh for further analyses. Convergence histories for the inviscid flow are shown in Figures 6 and 7 compare the computed viscous case surface pressure distribution with the experimental data [14] on NACA0012 with $M_\infty = 0.755$, $\alpha_m = 0.016^\circ$, $\alpha_p = 2.51^\circ$, $k = 0.0814$ for two angles of attacks. As it is seen from these results, there is quite a good agreement between the present method and the measurement of Landon [14]. These comparisons show that the solutions using oscillating boundary condition method has good prediction.

The computed variation of the lift coefficient versus angle of attack for inviscid and viscous flows during the third cycle is compared with that Landon [14] and Uzun [15] and in Figure 8. The existence of this variation loop is the result of induced velocities, which result in different lift coefficients between the up and down strokes. For presented viscous case, the turbulence quantities were specified at inlet to correspond to 0.008 turbulence intensity and a dissipation length scale of 10% of the airfoil chord. The value of K in SBIC scheme for this case is 0.3. Figure 8a shows the computed variation of lift coefficient versus angle of attack for viscous case which is in close agreement with experimental data. Because the flow around a pitching oscillation airfoil is disturbed and turbulence models can influence the results, the little difference between the numerical prediction and experimental data could be due to turbulence model. Figure 8b shows the C_l versus α for inviscid

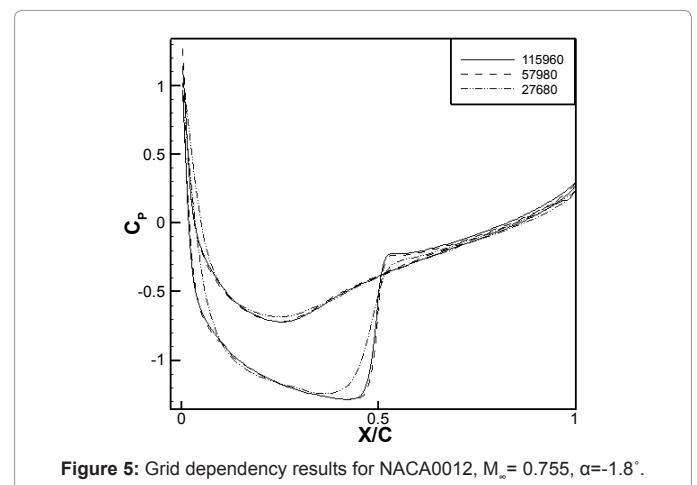


Figure 5: Grid dependency results for NACA0012, $M_\infty = 0.755$, $\alpha = -1.8^\circ$.

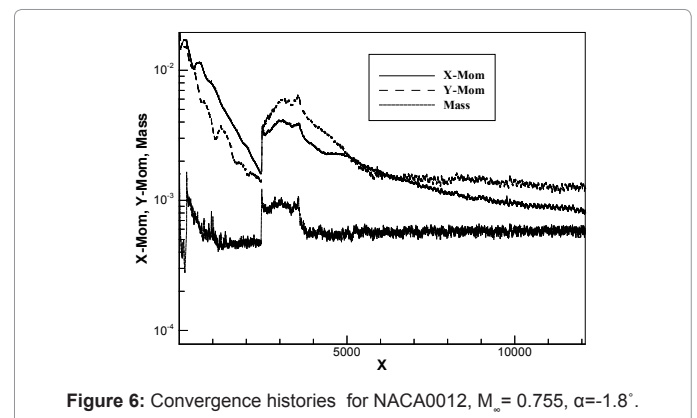
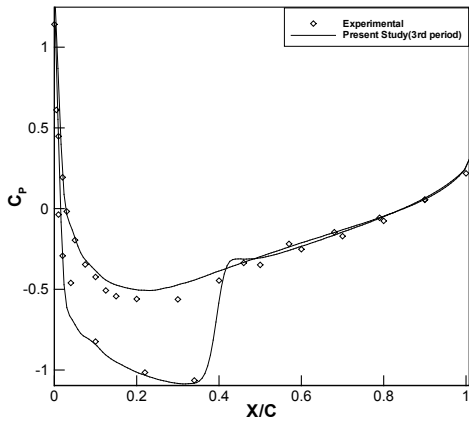
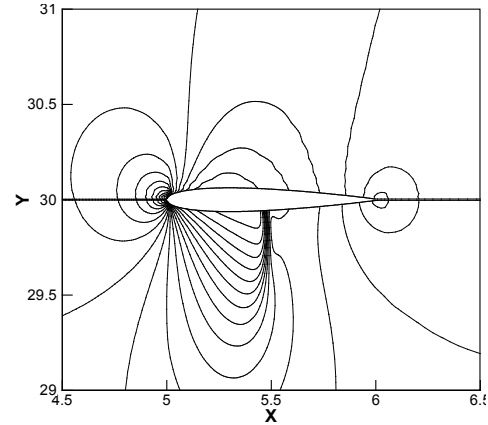


Figure 6: Convergence histories for NACA0012, $M_\infty = 0.755$, $\alpha = -1.8^\circ$.



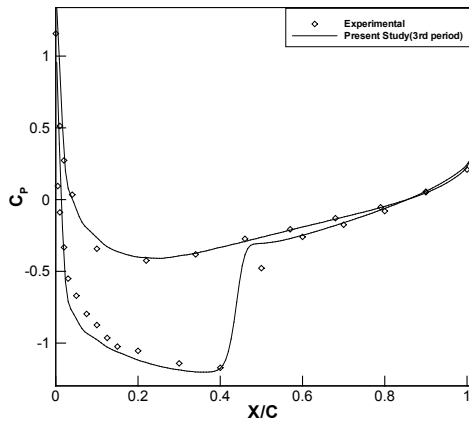
a: Pressure coefficient distribution

$$\alpha(t) = -0.54^\circ$$



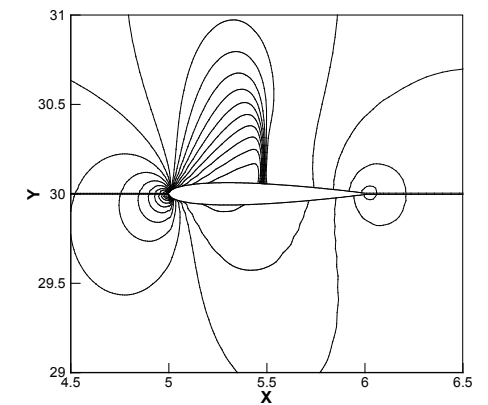
b: Pressure coefficient contours

$$\alpha(t) = -0.54^\circ$$



c: Pressure coefficient distribution

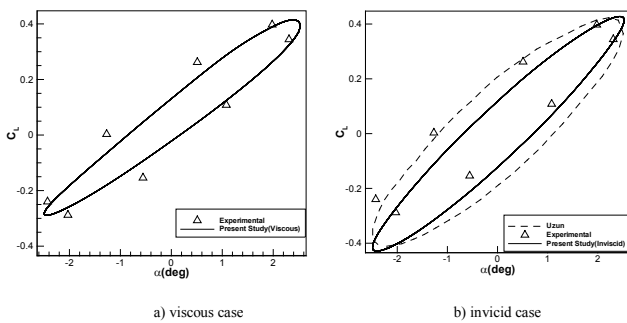
$$\alpha(t) = 2.34^\circ$$



d: Pressure coefficient contours

$$\alpha(t) = 2.34^\circ$$

Figure 7: Pressure distribution on NACA0012, $M_\infty=0.755$, $\alpha_m=0.016^\circ$, $\alpha_p=2.51^\circ$, $k=0.0814$.



a) viscous case

b) inviscid case

Figure 8: Lift coefficient versus angle of attack for $M_\infty=0.755$, $\alpha_m=0.016^\circ$, $\alpha_p=2.51^\circ$, $k=0.0814$.

case. Uzun [15] used a parallel algorithm for the solution of unsteady Euler equation on unstructured reformatting grids while this study

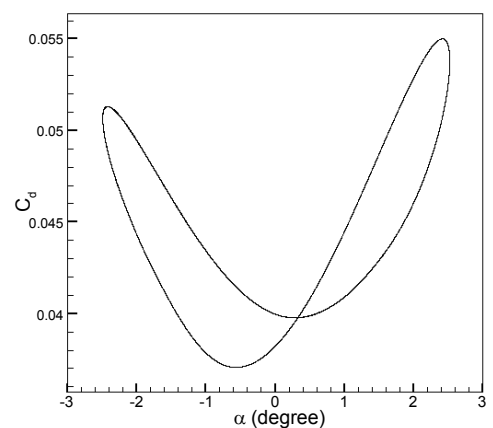
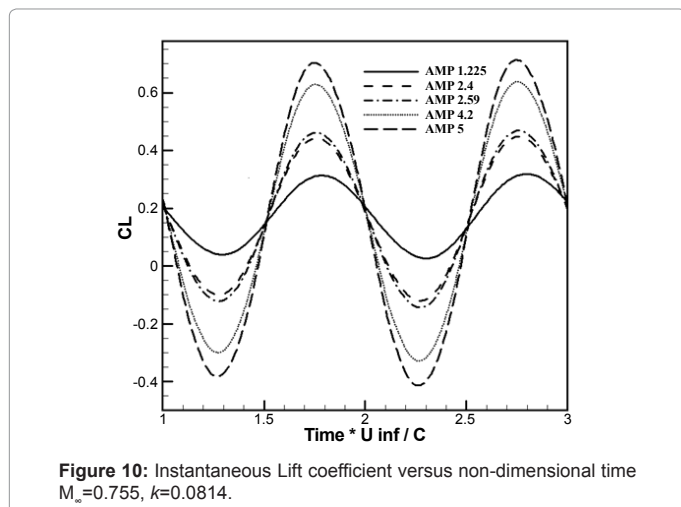


Figure 9: Drag coefficient versus angle of attack for viscous case at $M_\infty=0.755$, $\alpha_m=0.016^\circ$, $\alpha_p=2.51^\circ$, $k=0.0814$.



	Iterative Algorithm	Non-Iterative Algorithm	New Algorithm
Internal Loop No.	-	20-30	2-3
External Loop No.	1000		1-2
CPU Time (min)	8600	2800	120

Table 3: CPU Time comparison for different algorithms.

non moving mesh with oscillation of flow boundary condition is applied. It can be seen that both methods are not good agreement with experimental data particularly at the lowest angle of attack. The reason for this difference is caused by the lack of consideration of viscosity. In other words, the viscosity can effect on the separated vortex from the airfoil and aerodynamic coefficients in unsteady flow.

The predicted drag coefficients versus angle of attack are illustrated in Figure 9. The upstroke C_d and C_{dmin} are higher than the down stroke one. In this work, the effect of the airfoil amplitude of oscillation on the simulated lift coefficients is assessed. The instantaneous C_L versus τ where $K=0.0184, M=0.755$ on NACA0012 is indicated in Figure 10. As illustrated, the maximum lift coefficients increases at higher amplitudes of oscillation, the calculated lift coefficients are periodic and resemble harmonic-like patterns. Furthermore, increasing amplitude endues significant lead in the C_L results that C_{Lmax} is obtained at a lower τ . This can be attributed to the stronger effects of the shed wake and vertical structures on the surrounding fluid at the higher amplitudes. Table 3 indicate CPU Time comparison for different algorithms. The numbers of iteration to satisfy convergence criteria for the external loops of algorithms (a),(b) and (c) are approximately 10,000 and 1-2 respectively. For internal loops, the numbers of iterations of these algorithms are about 0, 20-30 and 2-3 respectively. As a result, the two algorithms (a) and (b) are time consuming and CPU time for new method is considerably decreased.

Conclusions

A pressure based implicit procedure to solve the Euler and Navier-Stokes equations is developed to predict transonic viscous and inviscid flows around the pitching airfoil with high resolution scheme. In order to simulate pitching airfoil, oscillation of flow boundary condition is applied. The boundedness criteria for this procedure are determined from Normalized Variable Diagram (NVD) scheme. The main findings can be summarized as follows: 1-The pitching airfoil simulation with the oscillation of flow boundary condition with fix grid is very simple and has low cost. 2-The grid dependence test with high resolution

scheme indicates that an acceptable solution can be obtained even on a fairly coarse 3-The agreement between numerical and experimental data is considerable. 4-The CPU time for new method considerably reduce.

References

- Feng D, Yizhao W, Xueqiang L (2007) Numerical Simulation of Two-Dimensional Unsteady Viscous Flow Based on Hybrid Dynamic Grids. Journal of Nanjing University of Aeronautics & Astronautics 39: 444-448.
- Tadghighi H, Liu Z, Ramakrishnan S (2005) A Pseudo Grid-Deformation Approach for Simulation of Unsteady Flow Past a Helicopter in Hover and Forward Flights. 43rd AIAA Aerospace Sciences Meeting and Exhibit 10-13 January Reno Nevada USA.
- Hao Z, Wei-qi Q (2007) Numerical simulation of gust response for airfoil and wing. Acta Aerodynamica Sinica 25: 531-536.
- Hao Z, Wei-qi Q (2009) Numerical simulation on gust response of elastic wing. Chinese Journal of Computational Mechanics 26: 270-275.
- Gopalan H, Povitsky A (2008) A Numerical Study of Gust Suppression by Flapping Airfoils. 26th AIAA Applied Aerodynamics Conference 18-21 August Honolulu, Hawaii.
- Raveh D (2010) CFD-Based Gust Response Analysis of Free Elastic Aircraft. ASD Journal 2; 23-24.
- Raveh DE (2011) Gust-Response Analysis of Free Elastic Aircraft in the Transonic Flight Regime. J Aircraft 48: 1204-1211.
- Raveh DE (2007) CFD-Based Models of Aerodynamic Gust Response. J Aircraft 44: 888-897.
- Sitaraman J, Baeder J, Iyengar V (2003) On the Field Velocity Approach and Geometric Conservation Law for Unsteady Flow Simulations. 16th AIAA Computational Fluid Dynamics Conference, USA.
- Yang ZY, Chin SB, Swithenbank J (1991) On the modelling of the k-equation for compressible flow. Proceedings of the 7th International Conference, Stanford, CA, USA.
- Narayan JR, Sekar B (1991) Computation of Turbulent High Speed Mixing Layers Using a Two-Equation Turbulence Model. Computational Fluid Dynamics Symposium on Aeropropulsion 409-428.
- Djavarehshkian MH (2004) Pressure-based compressible calculation method utilizing normalized variable diagram scheme. Iran J Sci Technol 28: 495-500.
- Issa RI (1986) Solution of the implicitly discretised fluid flow equations by operator-splitting. J Comput Phys 62: 40-65.
- Landon RH (1982) NACA0012 oscillation and transient pitching," in Compendium of Unsteady Aerodynamic Measurements, Advisory Report 702.
- Uzun, A (1999) Parallel Computations of Unsteady Euler Equations on Dynamically Deforming Unstructured Grid. M.Sc. Thesis Purdue University USA.